JOURNAL OF SPACECRAFT AND ROCKETS
Vol. 41, No. 2, March–April 2004

Engineering Notes

ENGINEERING NOTES are short manuscripts describing new developments or important results of a preliminary nature. These Notes cannot exceed six manuscript pages and three figures; a page of text may be substituted for a figure and vice versa. After informal review by the editors, they may be published within a few months of the date of receipt. Style requirements are the same as for regular contributions (*see inside back cover*).

Surface Recombination Coefficients and Boundary-Layer Hypersonic-Flow Calculations on Different Surfaces

I. Armenise*
Consiglio Nazionale delle Ricerche, 70126 Bari, Italy
M. Barbato†
Scuola Universitaria Professionale della Svizzera Italiana, CH-6928 Manno, Switzerland
and
M. Capitelli‡ and C. Gorse§
Bari University, 70126 Bari, Italy

Introduction

A state-to-state vibrational model describing molecules at different vibrational levels as different species has recently been developed to investigate the interaction of dissociating oxygen[1] and air[2] on SiO_2 in the boundary layer of an hypersonic vehicle.

State-selected rates of recombination of atomic species on SiO_2 surfaces into vibrationally excited molecules in the gas phase were obtained either by a molecular dynamic approach, in the case of oxygen, or by a phenomenological[3,4] one, in the case of air.

The phenomenological approach, however, disregarded all of the couplings between the different heterogeneous reactions occurring on the surface[3,5] and in particular their dependence on surface material, chemical species, and temperature.

This information will be included in our state-to-state model[1,2] and applied to metallic surfaces to investigate the effect of the catalyticity of different materials on concentrations and vibrational distributions of molecules in the boundary layers of reentry bodies.

Physical Model

The heterogeneous dissociation–recombination reactions included in the present model are[2]

$$\mathrm{N} + \mathrm{N}^* \xrightarrow{\gamma_{\mathrm{NN}}} \mathrm{N}_2(\mathrm{v}) + * \tag{1}$$

$$\mathrm{O} + \mathrm{O}^* \xrightarrow{\gamma_{\mathrm{OO}}} \mathrm{O}_2(\mathrm{v}) + * \tag{2}$$

$$\mathrm{O} + \mathrm{N}^* \xrightarrow{\gamma_{\mathrm{ON}}} \mathrm{NO} + * \tag{3}$$

$$\mathrm{N} + \mathrm{O}^* \xrightarrow{\gamma_{\mathrm{NO}}} \mathrm{NO} + * \tag{4}$$

and the corresponding recombination coefficients γ_{AB} have been obtained in Refs. 3 and 4. Here * is the active adsorption site and N^* and O^* are the ad-atoms.

These processes, together with those occurring in the gas phase,[2] have been inserted into the boundary-layer equations[2,6]

$$C_v'' + f \cdot Sc \cdot C_v' = S_v \tag{5a}$$

$$\Theta'' + f \cdot Pr \cdot \Theta' = S_T \tag{5b}$$

Here $C_v = \rho_v/\rho$, v is the species index, $\Theta = T/T_e$, e is the boundary layer external edge index, f is the stream function, and S_v and S_T are the source terms of the continuity equations and of the energy equation, respectively. The derivatives are taken with respect to the coordinate normal to the surface, η. The Prandtl and Schmidt numbers have been considered constant: $Pr = 0.71$, $Sc = 0.49$. Better results could be obtained by using one-dimensional boundary-layer equations including multicomponent diffusion coefficients.

Rate coefficients for the kinetic processes in both heterogeneous and homogeneous phases can be found in Refs. 2 and 7. The selected rates can be considered a judicious choice of the data existing in the literature: the accuracy for high-lying vibrational levels should be estimated to an order of magnitude, emphasizing the qualitative nature of the present results.

The surface processes described by Eqs. (1–4) enter into Eqs. (5) as boundary conditions for the derivative of each species[2]:

$$\left.\frac{\partial C_{\mathrm{N}}}{\partial \eta}\right|_w = \frac{\gamma_{\mathrm{NN}}}{D_{\mathrm{N}}}\sqrt{\frac{kT}{2\pi m_{\mathrm{N}}}} \cdot C_{\mathrm{N}} + \frac{\gamma_{\mathrm{NO}}}{D_{\mathrm{N}}}\sqrt{\frac{kT}{2\pi m_{\mathrm{N}}}} \cdot C_{\mathrm{N}} \tag{6a}$$

$$\left.\frac{\partial C_{\mathrm{N}_2}}{\partial \eta}\right|_w = -\frac{\gamma_{\mathrm{NN}}}{D_{\mathrm{N}}}\sqrt{\frac{kT}{2\pi m_{\mathrm{N}}}} \cdot C_N \tag{6b}$$

$$\left.\frac{\partial C_{\mathrm{O}}}{\partial \eta}\right|_w = \frac{\gamma_{\mathrm{OO}}}{D_{\mathrm{O}}}\sqrt{\frac{kT}{2\pi m_{\mathrm{O}}}} \cdot C_{\mathrm{O}} + \frac{\gamma_{\mathrm{ON}}}{D_{\mathrm{O}}}\sqrt{\frac{kT}{2\pi m_{\mathrm{O}}}} \cdot C_{\mathrm{O}} \tag{6c}$$

$$\left.\frac{\partial C_{\mathrm{O}_2}}{\partial \eta}\right|_w = -\frac{\gamma_{\mathrm{OO}}}{D_{\mathrm{O}}}\sqrt{\frac{kT}{2\pi m_{\mathrm{O}}}} \cdot C_{\mathrm{O}} \tag{6d}$$

$$\left.\frac{\partial C_{\mathrm{NO}}}{\partial \eta}\right|_w = -\frac{\gamma_{\mathrm{ON}}}{D_{\mathrm{O}}}\sqrt{\frac{kT}{2\pi m_{\mathrm{O}}}} \cdot C_{\mathrm{O}} - \frac{\gamma_{\mathrm{NO}}}{D_{\mathrm{N}}}\sqrt{\frac{kT}{2\pi m_{\mathrm{N}}}} \cdot C_{\mathrm{N}} \tag{6e}$$

It should be noted that according to the phenomenological approach of Ref. 2, heterogeneous recombination pumps vibrational energy to the tops of the vibrational ladders of N_2 and O_2.

The boundary conditions are completed by two constant temperatures, T_e and T_w, at the edge of the boundary layer and at the body surface, respectively. Boltzmann vibrational distributions and chemical equilibrium are generally assumed at the edge of the boundary layer.

Numerical Method

Equations (5a) and (5b) are solved using an iterative approach along the self-similar[6,7] coordinate η.

Received 8 July 2002; revision received 2 December 2003; accepted for publication 2 December 2003.

*Researcher, Istituto di Metodologie Inorganiche e dei Plasmi, Via Orabona 4; i.armenise@area.ba.cnr.it.

†Senior Researcher, Dipartimento di Elettronica e Informatica, Via Cantonale Galleria 2; barbato@die.supsi.ch.

‡Full Professor, Chemistry Department, Via Orabona 4; also Section Head, Istituto di Metodologie Inorganiche e dei Plasmi, Consiglio Nazionale delle Ricerche, Via Orabona 4, 70126 Bari, Italy; m.capitelli@area.ba.cnr.it. Associate Fellow AIAA.

§Full Professor, Chemistry Department, Via Orabona 4; c.gorse@area.ba.cnr.it.

The distance along the η coordinate is divided into 80 points and the equations are discretized using central differences. The grid convergence has been tested by running the code for particular conditions ($T_e = 7000$ K, $P_e = 1000$ N/m^2, $T_w = 1000$ K, SiO_2 surface) on three different grids (80, 160, and 320 points). The Richardson extrapolation obtained from these three sets of results has been used to verify the χ^2 test:

$$\chi^2 = \sum_{i=1}^{n} \frac{(O_i - \mathrm{RE}_i)^2}{\mathrm{RE}_i}$$

where n is the number of points considered, RE_i represents the Richardson extrapolation value on point i, and O_i is the value calculated at point i. This test gives the accuracy of the whole distributions of the different quantities [$N_2(v)$, $O_2(v)$, N_2, N, O_2, O, NO, T]. The χ^2 values are in all cases much less than n, thus indicating that our choice of 80 points gives a good approximation to the distributions. As an example, for SiO_2, the χ^2 values for the species N_2, N, O_2, O, and NO are, respectively, 1.5, 0.6, 0.3, 0.8, and 1.1×10^{-2}.

The improvements implemented in the code concern the chemical species boundary conditions [Eqs. (6)]. In particular, the recombination coefficients γ are updated at each iteration during the solution procedure.

The update process works according to the following steps: 1) at iteration n the up-to-date concentrations are used to evaluate the

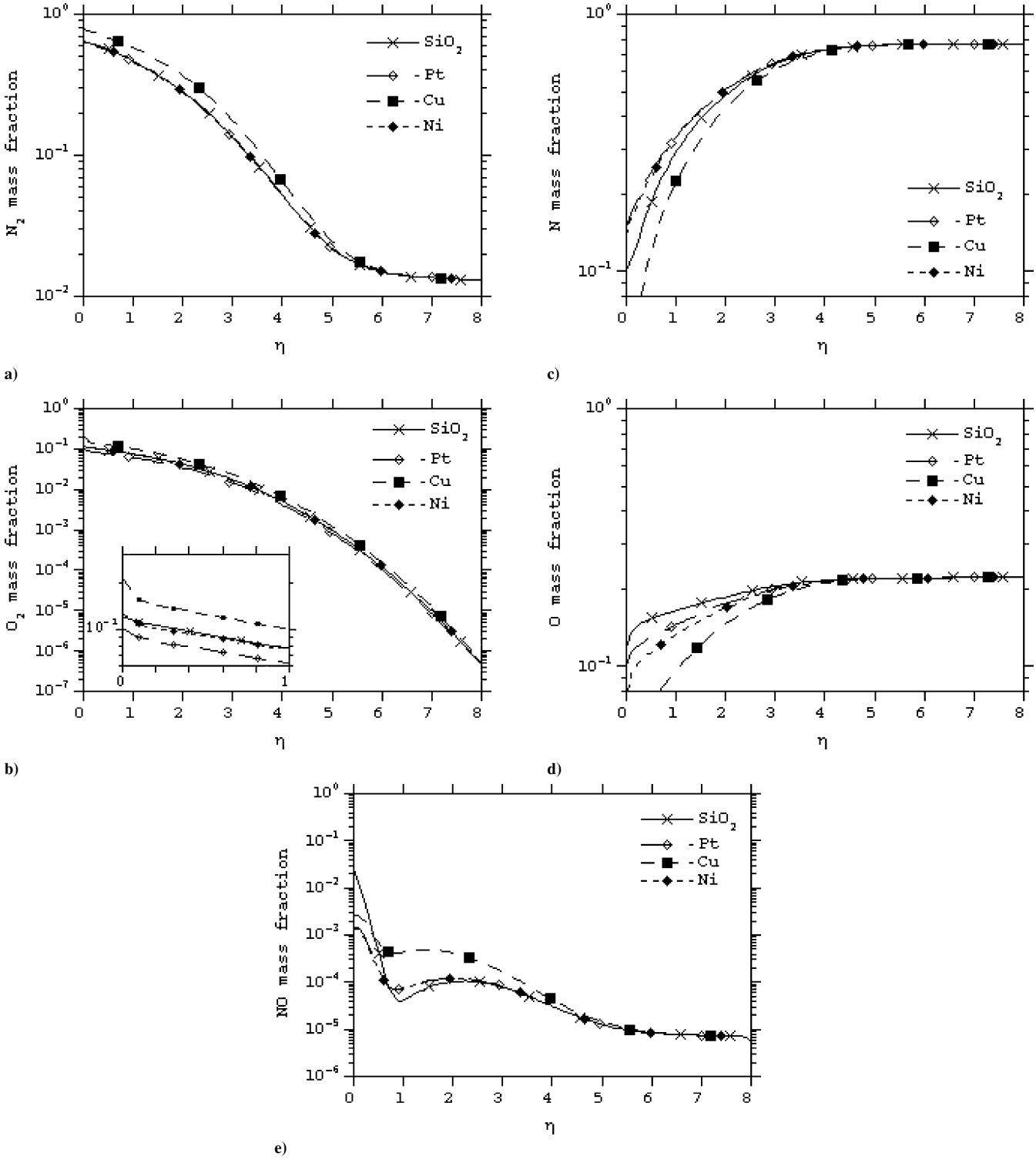

Fig. 1 Mass fractions along η for different surfaces: a) N_2, b) O_2, c) N, d) O, and e) NO.

nitrogen and oxygen ad-atom concentrations; 2) the updated ad-atom concentrations are then used to calculate the recombination coefficients γ for all of the molecular species; 3) the updated values of recombination coefficients γ are inserted into the finite rate catalysis boundary conditions [see Eqs. (6)]; 4) solution step $n+1$ is then performed and the new concentrations are calculated; and 5) the process is repeated until the relative differences of the mass fractions of two consecutive iterations do not exceed 10^{-4}.

The differences between the present results and those of Ref. 2 for a SiO_2 surface do not exceed a factor of 2.

Results

We present results for SiO_2 and for Pt, Cu, and Ni metallic surfaces for the same conditions discussed in our previous works,[1,2] i.e., $T_e = 7000$ K, $P_e = 1000$ N/m^2, and $T_w = 1000$ K. The vibrational distribution and the chemical composition at the edge of the boundary layer are calculated at T_e by considering thermal equilibrium.

Figures 1a–1e illustrate the behavior of the different species mass fractions as functions of η.

In particular, Figs. 1a and 1b show the N_2 and O_2 mass fractions. The molecular-species mass fractions do not appreciably depend on the selected material, which on the contrary affects the atomic-species mass fractions (Figs. 1c and 1d). Cu is the most active catalyst, producing almost complete consumption of the atomic species on the surface ($\eta = 0$). The atomic-oxygen mass fractions reflect the magnitude of the catalytic activities, whereas the atomic-nitrogen mass fractions shown in Fig. 1c indicate that the consumption of this species is larger for SiO_2 than for Pt and Ni. This result is due to the neglect of NO formation on metallic surfaces. On the other hand, the catalytic formation of NO on SiO_2 indirectly increases the N-atom heterogeneous-reaction coefficients with respect to a surface on which N atoms can react to form only N_2. For the metal-surface model, this fact represents, at the moment, a limitation that can be removed once a more suitable set of data are available, and we believe that this could affect the final results. An estimate of this effect can be obtained by eliminating the NO recombination process on a SiO_2 surface. Comparison of the different quantities calculated, including or omitting the process, shows differences up to a factor of 2.

Finally, the NO mass fractions shown in Fig. 1e feature non-negligible variations according to the material selected and to the assumptions about the NO catalytic formation.

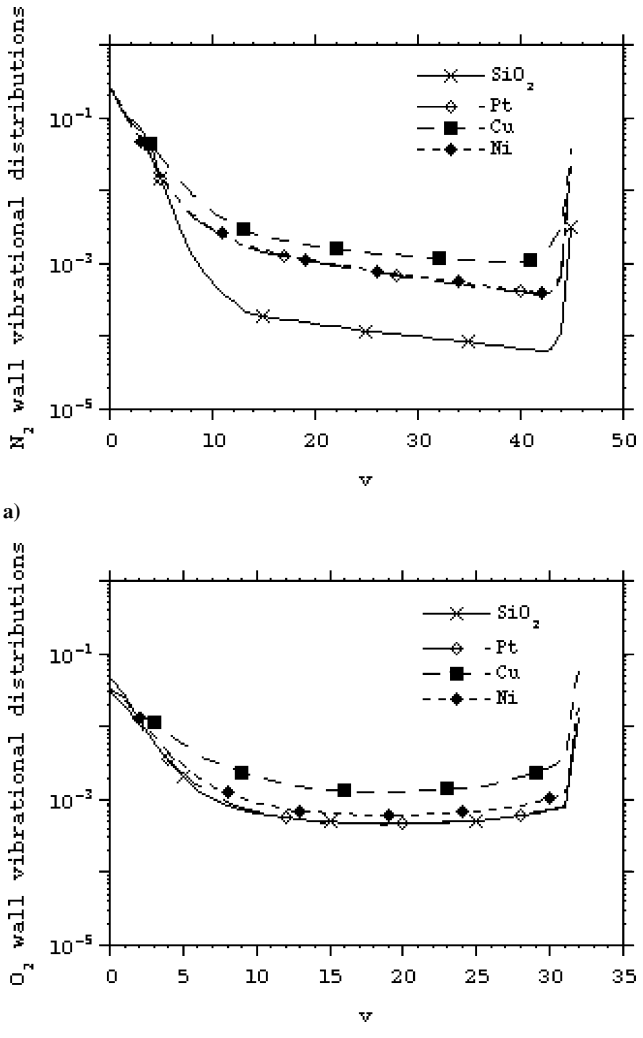

Fig. 2 Wall ($\eta = 0$) vibrational distributions vs the vibrational level v for different surfaces: a) N_2 and b) O_2.

Figures 2a and 2b illustrate the vibrational distributions of N_2 (Fig. 2a) and O_2 (Fig. 2b) on SiO_2 and metallic surfaces. An order-of-magnitude increase of the vibrational distribution near the metallic surfaces is evident when compared with the results corresponding to SiO_2 (see Figs. 2a and 2b). The peaks on the last vibrational level are due to the chosen surface-recombination model, which considers the recombination occurring on the last vibrational level of the molecule (both N_2 and O_2).

The results reported so far have been obtained by assuming thermal equilibrium at the edge of the boundary layer. However, complete equilibration of translational and vibrational temperature and chemistry at T_e depend on the reentry conditions. We can define for a given translational temperature T_e different vibrational temperatures at the edge of the boundary layer ($T_{e,\mathrm{vib}}$) and different chemical equilibrium at $T_{e,\mathrm{vib}}$. To study the effect of the different temperatures at the boundary-layer edge we have run our code parameterizing T_e and $T_{e,\mathrm{vib}}$. The results for the vibrational distributions of N_2 and O_2 near to the surface show the persistence of the plateau for molecular oxygen for all examined $T_{e,\mathrm{vib}}$ even though at low $T_{e,\mathrm{vib}}$ ($T_{e,\mathrm{vib}} \leq 2000$ K) the plateau is limited to high-lying levels. The situation for nitrogen is more complex due to the formation of NO from N_2 and oxygen atoms. Clear evidence of the N_2 plateau occurs in this case for $T_{e,\mathrm{vib}} > 6000$ K.

Conclusions

Heterogeneous catalytic-recombination coefficients depending on the local flow conditions, i.e., temperature and chemical-species partial pressures, have been implemented into a one-dimensional boundary-layer code that includes state-to-state vibrational kinetics.

The model has been applied to different metallic surfaces and produces large differences in the mass fractions and vibrational distributions, depending on the material selected. Cu surfaces present the largest effects.

In conclusion, the most important point of the present calculations is the clear evidence of the existence of nonequilibrium vibrational distributions near ceramic and metallic surfaces.

Acknowledgment

This work has been partially supported by the Agenzia Spaziale Italiana, I/C/251/01/0, Subcontract CSPA.ATD.SC.02.03.

References

[1]Armenise, I., Capitelli, M., Gorse, C., Cacciatore, M., and Rutigliano, M., "Nonequilibrium Vibrational Kinetics of a O_2/O Mixture Hitting a Catalytic Surface," *Journal of Spacecraft and Rockets*, Vol. 37, No. 3, 2000, pp. 318–323; also AIAA Paper 99-3631, June–July 1999.

[2]Armenise, I., Capitelli, M., and Gorse, C., "Nonequilibrium Vibrational Kinetics of Air Hitting a Catalytic SiO_2 Surface," *Journal of Spacecraft and Rockets*, Vol. 38, No. 4, 2001, pp. 482–487.

[3]Nasuti, F., Barbato, M., and Bruno, C., "Material-Dependent Catalytic Recombination Modeling for Hypersonic Flows," *Journal of Thermophysics and Heat Transfer*, Vol. 10, No. 1, 1996, pp. 131–136.

[4]Barbato, M., Reggiani, S., Bruno, C., and Muylaert, J., "Model for Heterogeneous Catalyis on Metal Surfaces with Applications to Hypersonic Flows," *Journal of Thermophysics and Heat Transfer*, Vol. 14, No. 3, 2000, pp. 412–420.

[5]Fertig, M., Fruhauf, H. H., and Auweter-Kurtz, M., "Modelling of Reactive Processes at SiC Surfaces in Rarefied Nonequilibrium Airflows," AIAA Paper 2002-3102, June 2002.

[6]Armenise, I., Capitelli, M., Colonna, G., Koudriavtsev, N., and Smetanin, V., "Nonequilibrium Vibrational Kinetics During Hypersonic Flow of a Solid Body in Nitrogen and Its Influence on the Surface Heat Flux," *Plasma Chemistry and Plasma Processing*, Vol. 15, No. 3, 1995, pp. 501–528.

[7]Capitelli, M., Armenise, I., and Gorse, C., "State-to-State Approach in the Kinetics of Air Components Under Re-Entry Conditions," *Journal of Thermophysics and Heat Transfer*, Vol. 11, No. 4, 1997, pp. 570–578.

B. Hassan
Associate Editor

International Space Station Ku-Band Communications Antenna Blockage Analysis

Shian U. Hwu* and Yin-Chung Loh†
Lockheed Martin Space Operations, Houston, Texas 77258
and
Quin D. Kroll‡ and Catherine C. Sham§
NASA Johnson Space Center, Houston, Texas 77258

Introduction

THE International Space Station (ISS) is a large and complex spacecraft. The solar panels and thermal radiators are rotated dynamically to maintain a preferential orientation with respect to the sun. The space station Ku-band antenna tracks the geostationary Tracking Data and Relay Satellite (TDRS) and will encounter blockage from the space station structures, especially the solar panels and the thermal radiators, as shown in Fig. 1. These blockages may cause communication outages and reduce communication quality. An understanding of blockage effects is necessary for prediction of communication coverage. The ISS Ku-band antenna is a 2-m-diam reflector antenna. The antenna's operating frequencies are 15.0034 GHz for transmitting and 13.775 GHz for receiving. The previous ISS Ku-band antenna model for communication coverage analysis is very conservative.[1] This conservative approach is based on International Space Station/Shuttle reflector antenna test data. Additional computer simulation and test results indicate that in the near field, the energy radiated by the reflector antenna is mostly confined within the antenna aperture projected cylinder.[2] The Ku-band communication link was assumed to be lost if the 2-m-aperture projected cylinder was blocked by any ISS structures. If the antenna's aperture projected cylinder is clear of any structure blockage, the multipath degradation from ISS structures is insignificant. The communication link will not be subject to much impact from the ISS structure multipath effects.

Recently obtained uplink flight data indicate that the 2-m-diam cylinder model is too conservative.[1] Flight data indicate that the Ku-band antenna can track the TDRS satellite with partial solar panel or thermal radiator blockage. The data indicate that the ISS Ku-band link can sustain 4.6 dB signal-power-level degradation (relative to the signal power without structure blockage at maximum slant range to TDRS) before the software controller forces the communication link to drop. As a result of the 4.6-dB available margin, partial blockage to the ISS Ku-band reflector antenna should be allowed in the Ku-band communication coverage analysis to better reflect the actual communication link margin and coverage performance. The following simulation and analysis were performed to improve the previously used conservative approach to better predict the actual communication performance.

Signal Strength Computations

In the communication system performance simulations, the ISS Ku-band reflector antenna is modeled by a set of equivalent dipoles. The reflector antenna aperture fields are computed and then converted to a set of equivalent dipoles. The equivalent dipoles are used as the equivalent radiation sources of the ISS Ku-band reflector antenna. The solar panels and thermal radiators are modeled as perfect conducting plates. The solar array panel is a composite structure formed by closely spaced solar cells. The solar cells are made of silicon and are welded onto the front surface of the solar array panel. A grid of copper strips that collect current is on the back side of the solar array panel. To characterize the scattering properties of the solar array panels, experimental investigations were performed at Ku-band frequencies. Based on the results obtained, the solar array panels exhibit scattering properties similar to those of a conducting panel of the same size.[1] The solar array panels were modeled approximately using perfect reflecting plates at Ku-band frequencies.

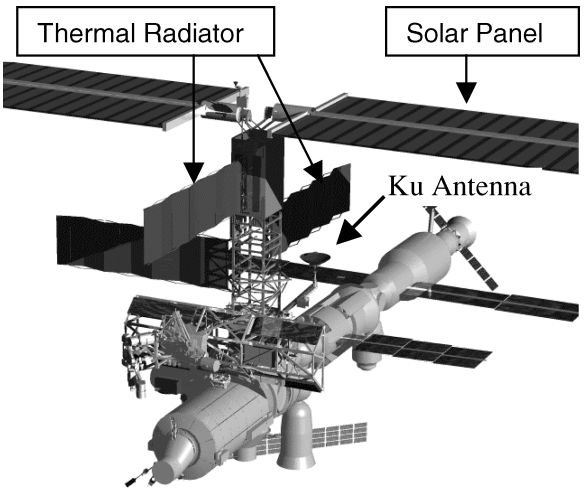

Fig. 1 Ku-band antenna will encounter solar panel and thermal radiator blockage.

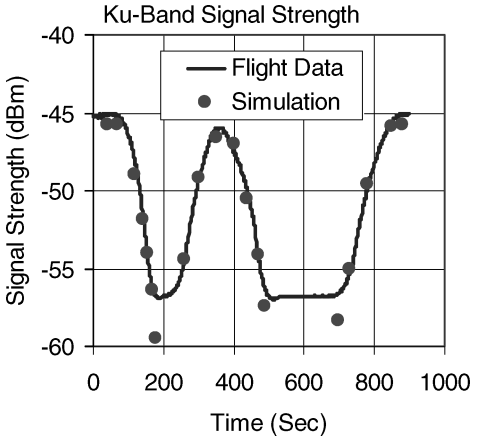

Fig. 2 Computed signal strength compared with flight data along a selected TDRS satellite path with solar panel blockage.

Received 14 April 2003; revision received 16 December 2003; accepted for publication 16 December 2003.

*Senior Staff Engineer, Avionics Systems Analysis Section, 2400 NASA Road 1. Senior Member AIAA.

†Section Manager, Avionics Systems Analysis Section.

‡Project Engineer, Systems Analysis and Verification Branch, MC: EV7, 2101 NASA Road 1.

§Deputy Branch Chief, Systems Analysis and Verification Branch, MC: EV7, 2101 NASA Road 1.